

Research



Cite this article: Li Y, Cai R, Lü R, Gao L, Qin S. 2018 Template synthesis of the Cu₂O nanoparticle-doped hollow carbon nanofibres and their application as non-enzymatic glucose biosensors. *R. Soc. open sci.* **5**: 181474. <http://dx.doi.org/10.1098/rsos.181474>

Received: 27 September 2018

Accepted: 25 October 2018

Subject Category:

Chemistry

Subject Areas:

inorganic chemistry/materials science/
nanotechnology

Keywords:

template synthesis, Cu₂O nanoparticles, doped,
hollow carbon nanofibres, biosensors

Author for correspondence:

Renjiang Lü

e-mail: lvrenjiang123@163.com

This article has been edited by the Royal Society of Chemistry, including the commissioning, peer review process and editorial aspects up to the point of acceptance.

Electronic supplementary material is available online at <https://doi.org/10.6084/m9.figshare.c.4304246>.



Template synthesis of the Cu₂O nanoparticle-doped hollow carbon nanofibres and their application as non-enzymatic glucose biosensors

Yingjie Li, Renhao Cai, Renjiang Lü, Lidi Gao
and Shili Qin

College of Chemistry and Chemical Engineering, Qiqihar University, Qiqihar, Heilongjiang 161006, People's Republic of China

RC, 0000-0002-1791-5544

The cuprous oxide nanoparticle (Cu₂O NP)-doped hollow carbon nanofibres (Cu₂O/HCFs) were directly synthesized by the anodic aluminium oxide (AAO) template. The doped Cu₂O NPs were formed by *in situ* deposition by direct reduction reaction of precursor carbonization in thermal decomposition and could act as functionalized nanoparticles. The synthesized Cu₂O/HCFs were characterized in detail by transmission electron microscopy (TEM), scanning electron microscopy (SEM), X-ray diffraction (XRD), X-ray photoelectron spectroscopy (XPS), Raman spectroscopy and inductively coupled plasma mass spectrometry (ICP-MS). The results reveal that Cu₂O/HCFs have a tubular structure with an average diameter of approximately 60 nm. The shape of the Cu₂O/HCFs is straight and Cu₂O NPs are uniformly distributed and highly dispersed in HCFs. Cu₂O/HCFs have good dispersibility. The electrochemical activity of Cu₂O/HCFs was investigated by cyclic voltammetry (CV), the glucose sensors display high electrochemical activity towards the oxidation of glucose. Cu₂O/HCFs can effectively accelerate the transmission of electrons on the electrode surface. Cu₂O/HCFs are applied in the detection of glucose with a detection limit of 0.48 μM, a linear detection range from 7.99 to 33.33 μM and with a high sensitivity of 1218.3 μA cm⁻² mM⁻¹. Moreover, the experimental results demonstrate that Cu₂O/HCFs have good stability, reproducibility and selectivity. Our results suggest that Cu₂O/HCFs could be a promising candidate for the construction of non-enzymatic sensor.

1. Introduction

Owing to the special structure, good stability, unique electronic properties and the extraordinary mechanical properties, carbon-based materials have attracted considerable attention since they were discovered, and are widely used in many important technological fields such as catalysis [1], sensors [2], adsorbents [3] and electronic devices [4]. Among numerous carbon-based materials, one-dimensional hollow carbon-based materials have attracted more and more scientific and technological interest owing to their excellent properties such as high aspect ratio, light weight, high thermal conductivity, excellent electroconductibility and other superior characteristics [5].

To improve the practical application of one-dimensional materials, in recent years, researchers have combined metal and metal oxides with one-dimensional carbon-based materials [6,7]. The incorporation of metal or metal oxide nanoparticles with one-dimensional carbon-based materials may produce the synergistic effects and may lead to the improved property of the composites [8,9]. At present, such studies have been reported. For example, Zn ferrite/multi-walled carbon nanotube (Zn ferrite/MWCNT) composite was prepared [10]. The Zn ferrite/MWCNT composite showed the addition of low amount, low coating thickness and enhanced EM-wave absorption performance. Unique morphology $\text{Fe}_3\text{O}_4/\text{Fe}$ -carbon nanotube (CNT) nanocomposites at room temperature by a facile chemical synthesis method [11]. The capacitance of Fe_3O_4 could be extremely improved by dual conduction system containing CNTs and Fe. Ni-TiO₂/carbon nanotube photocatalysts were synthesized by a simple method [12]. The CNTs could be applied as useful photocatalytic support for the fixation of TiO₂. Hydrogen evolution was enhanced by the Ni loading on the TiO₂ nanocrystallites supported on the carbon nanotube. Combined metal or metal oxides with one-dimensional carbon-based materials have attracted more and more scientific interest.

Among various metal oxides, Cu₂O, as an important class of p-type semiconductor, has been paid much attention in enzyme-free glucose sensors in recent years owing to its high electrocatalytic activity, low cost and good stability, and it is a promising candidate in the fabrication of electrochemical materials, [13] and advantages of Cu₂O have been intensively investigated [14]. For example, the Cu/Cu₂O nanocluster-deposited carbon spheres have been synthesized through a layer-by-layer assembly method and subsequent *in situ* self-reduction process. The results showed that the Cu/Cu₂O nanoclusters are homogeneously anchored onto the carbon spheres. The double-shelled Cu/Cu₂O/CSs showed remarkable electrocatalytic activity toward glucose oxidation including two linear ranges with high selectivity of 63.8 and 22.6 $\mu\text{A cm}^{-2} \text{mM}^{-1}$ as well as good stability and repeatability [15]. Yazid *et al.* reported a highly sensitive and selective glucose sensor based on cuprous oxide/graphene nanocomposite-modified glassy carbon electrode (Cu₂O/graphene/GCE). The proposed sensor was successfully applied for the determination of glucose concentration in real human blood samples [16]. A type of nanospindle-like Cu₂O/straight multi-walled carbon nanotube (SMWNT) nanohybrid-modified electrode for sensitive enzyme-free glucose detection has been fabricated, the as-prepared nanospindle-like Cu₂O/SMWNT nanohybrids exhibit much higher electrocatalytic activity on the oxidation of glucose than the SMWNTs or Cu₂O alone as the electrode-modifying material. More importantly, the nanohybrid-modified electrodes also show good stability, reproducibility and high resistance against poisoning by chloride ion and the commonly interfering species such as ascorbic acid, dopamine, uric acid and acetamidophenol. These good analytical performances make the nanospindle-like Cu₂O/SMWNT nanohybrids promising for the future development of enzyme-free glucose sensors [17].

Recently, research on Cu₂O-doped carbon-based materials has gradually increased. Various morphologies of Cu₂O-doped carbon-based materials have been prepared by several different methods, such as chemical vapour deposition method, hydrothermal method, solvothermal method and wet chemical method [18–22]. These materials show excellent performance in solar cells, sensors and catalysis and other fields; however, there are some defects, such as uneven nanoparticle size, poor dispersion, carbon nanotube agglomeration and other issues. The unique structure of anodic aluminium oxide (AAO) template makes them very promising hosts for preparing one-dimensional nanomaterials. The precursor has been applied to backfill the template, which has resulted in the formation of one-dimensional nanostructures. Considering the composition of AAO template, it is believed that metal doped or decorated in the prepared one-dimensional nanostructures would be obtained through the *in situ* deposition reaction of AAO template. Therefore, we require a careful synthetic strategy to fabricate Cu₂O-doped HCFs with a high surface-to-volume ratio and expect to improve the electrochemical activity of HCF film enzyme-free glucose sensors, which is still a challenging work.

Herein, we have proposed a simple and effective technique for preparing novel hollow carbon nanofibres (HCFs) with highly dispersed Cu₂O nanoparticles by using the one-step direct AAO template route, which employed glucose as the carbon source and copper acetate (CuAc₂) as the

dopants. To investigate the structure and morphology of $\text{Cu}_2\text{O}/\text{HCFs}$, scanning electron microscopy (SEM), transmission electron microscopy (TEM), X-ray diffraction (XRD), Raman spectra and X-ray photoelectron spectroscopy (XPS) were carried out. Cyclic voltammetry (CV) was used to evaluate the electrochemical detection of the $\text{Cu}_2\text{O}/\text{HCFs}$ -modified electrode towards glucose.

2. Material and methods

2.1. Materials

Glucose, phosphoric acid, Na_2CO_3 and HNO_3 (AR, Kermel Ltd, China); copper acetate and perchloric acid (AR, Aladin Ltd, China); sodium hydroxide (AR, Jinli Ltd, China), high purity aluminium (99.999%, Mengtaiyouyan Technology Development Center, China); anhydrous ethanol (AR, Fuyu Fine Chemical Ltd, China) were used.

2.2. The preparation of AAO template

AAO templates were prepared by two-step anodization. High purity (99.999%) aluminium plates were ultrasonically cleaned in the mixed solution of acetone and alcohol ($v/v = 1:1$) for 30 min. All aluminium plates were annealed at 500°C for 2 h in a conventional furnace and degreased with acetone. The high purity aluminium plates were anodized in a 0.3 M oxalic acid solution under an applied voltage of 40 V and at a temperature around 4°C for 6 h. After accomplishing the first anodizing stage, alumina layers were removed by wet etching in aqueous solution of 6 wt% phosphoric acid and 1.8 wt% chromic acid at 70°C for 20 min. The textured Al plates were anodized again for 72 h under the same conditions as for the first anodizing. A subsequent etching treatment was carried out in a 6 wt% phosphoric acid solution at $40\text{--}50^\circ\text{C}$ for 1 h, followed by washing and drying.

2.3. The preparation of $\text{Cu}_2\text{O}/\text{HCFs}$

Glucose (10.00 g) and different mass CuAc_2 (0.50, 1.00, 2.00 and 4.00 g) were dissolved in 100 ml deionized water to obtain the corresponding precursors, the fabricated precursors were labelled as H-1, H-2, H-3 and H-4, respectively. After magnetic stirring for 30 min, the AAO membranes on Al substrate were placed in a home-made device, with the precursor in a separating funnel, and the reactor was subsequently evacuated. After opening the funnel cock, the nano-channels of the AAO templates were filled with the precursor depending on the atmospheric pressure. The templates were then removed from the vacuum container. After drying at room temperature for 6 h in an ambient environment and removal of surface residues [23], the templates were calcined in the N_2 atmosphere for 3 h at different temperatures (400, 500 and 600°C). After slow cooling to room temperature, the $\text{Cu}_2\text{O}/\text{HCFs}$ were obtained after removing the alumina template by etching with the 6 M NaOH solution.

2.4. The preparation of $\text{Cu}_2\text{O}/\text{HCFs}/\text{GCE}$

The modified electrode was prepared as follows. Five microlitres of the suspension with dispersed $\text{Cu}_2\text{O}/\text{HCFs}$ was coated on the pre-treated glassy carbon electrode and dried at room temperature. Before modification, the bare GCE was polished with 1, 0.5 and $0.03\ \mu\text{m}$ alumina slurry and then washed ultrasonically in deionized water, 50% (v/v) HNO_3 solution, ethanol and water for 6 min [24].

2.5. Electrochemical measurements

Electrochemical measurements were carried out on a CHI660E Electrochemical Workstation with a conventional three-electrode system composed of a platinum wire as an auxiliary electrode, a saturated $\text{Hg}/\text{Hg}_2\text{Cl}_2$ (SCE) as a reference electrode [15] and the modified electrode as a working electrode.

3. Results

Thermogravimetric (TG) curves of the precursor are displayed in figure 1. They revealed that the obvious weight loss occurred from room temperature to 170, 170 to 260 and 260 to 550°C . The first step of 5% weight loss corresponds to the evaporation of water from the precursor, and the second step of 13%

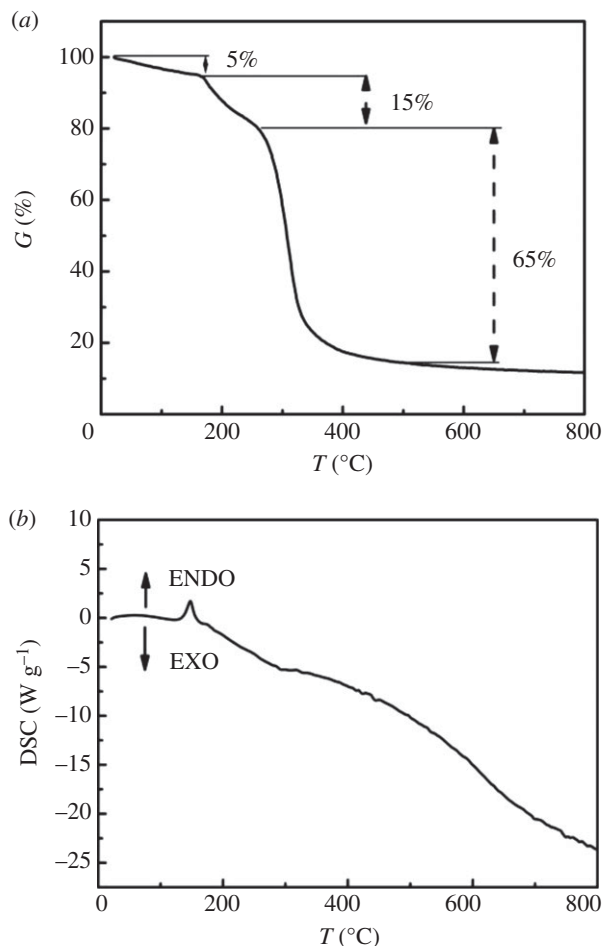


Figure 1. TG (a) and DSC (b) thermoanalytical response curves of precursor.

weight loss contributes to complete decomposition of copper acetate at the higher temperature with their corresponding endothermic peaks, which is in agreement with the composition of the precursor, as shown in the following reaction equation:



The third step of 65% weight loss for precursor may be due to the decomposition of glucose in the precursor. Above 550°C, the weight loss of the precursor remains unchanged. Glucose reduces CuO to Cu₂O. According to the TG data, 600°C was used as the calcination temperature of the products.

The surface morphologies of the as-synthesized Cu₂O/HCFs as imaged by SEM are shown in figure 2*a,b*. It can be observed from the photos that the carbon nanomaterials are overlapped with each other to form a large-area reticular morphology, the carbon nanomaterial is uniform in size, and the shape is straight. The prepared samples have a fibre structure with the uniform outer diameter of approximately 60 nm. The diameter and length of the samples mainly depend upon the porous nature of the AAO membrane (SEM images of the top view, electronic supplementary material, figure S1). Figure 2*c,d* shows the TEM images of Cu₂O/HCFs. One can see that almost all the Cu₂O/HCFs are hollow structures and have good monodispersity. Cu₂O NPs in the HCFs are highly dispersed and have no aggregation and the average size of Cu₂O NPs is about 21.5 nm. SEM and TEM display Cu₂O/HCFs outside the diameter, from which the average diameter of Cu₂O/HCFs can be 60 nm. This diameter is consistent with the pore diameter of the AAO templates.

The crystal structure of the as-synthesized catalysts was analysed by the XRD technique and their patterns of calcination at different temperatures are given in figure 3. All relatively intense diffraction peaks with 2θ angles of 36.2°, 43.5°, 62.4° and 74.7° correspond to the crystal planes of (111), (200), (220) and (311) of Cu matching well with the standard XRD pattern for Cu₂O of face-centred cubic lattice [25]. No peaks of impurity (such as Cu) were found in the XRD patterns, indicating that the obtained particles are pure cubic phase Cu₂O with high crystallinity. It must also be mentioned that

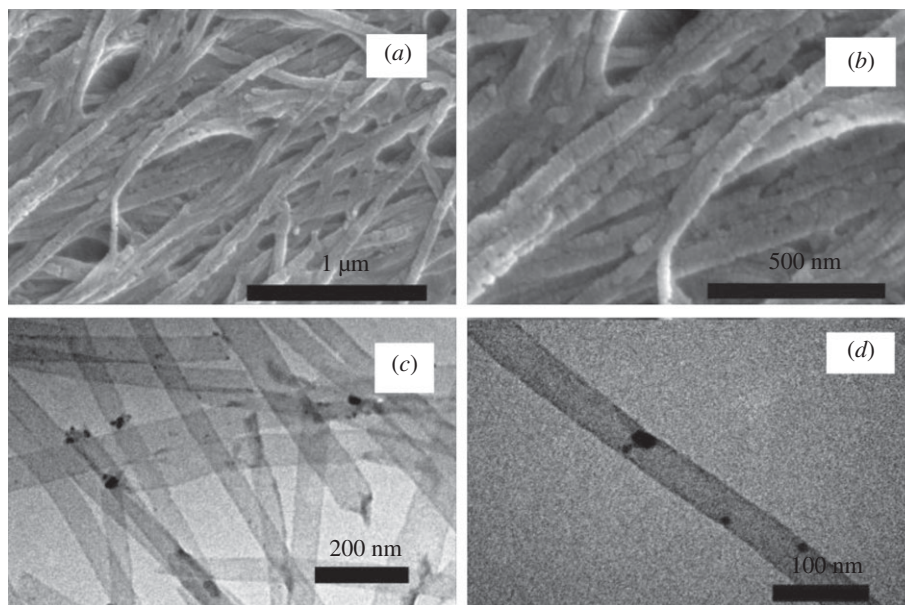


Figure 2. SEM images of the $\text{Cu}_2\text{O}/\text{HCFs}$: (a) large-area view and (b) small-area view, TEM images of the $\text{Cu}_2\text{O}/\text{HCFs}$: (c) lots of $\text{Cu}_2\text{O}/\text{HCFs}$, (d) a single $\text{Cu}_2\text{O}/\text{HCFs}$.

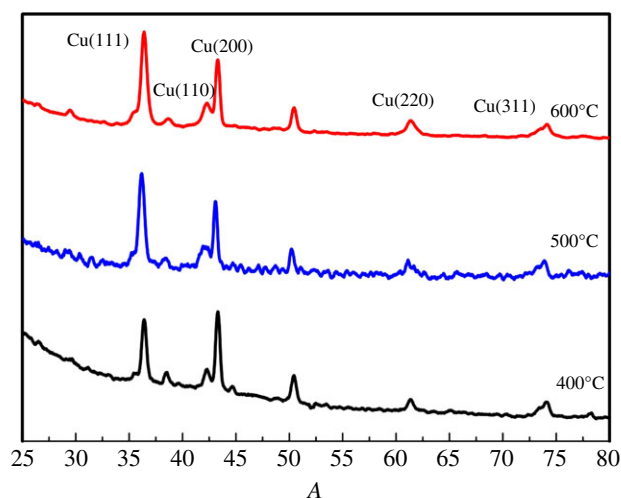


Figure 3. XRD patterns of $\text{Cu}_2\text{O}/\text{HCFs}$. Those were prepared at 400, 500 and 600°C for $\text{Cu}_2\text{O}/\text{HCFs}$.

the peaks broaden obviously; this indicates that smaller Cu_2O nanoparticles were formed in HCFs. The characteristic diffraction peak of graphitized carbon was found at 2θ angles of 26.02° and 42.3° ; according to the literature [26], the (002) (100) crystal face was assigned to carbon. Owing to the decomposition of glucose in the precursor to form hollow carbon nanostructures after high temperature calcination, Cu_2O nanoparticles appear in HCFs. The crystallite size was around 21.5 nm using the Scherrer formula; this is consistent with the observation from TEM. Figure 4 shows the Raman spectra of the samples calcined at 400, 500 and 600°C. The spectrum of our sample contains G band at 1584 cm^{-1} and D band at 1352 cm^{-1} . The D band represents the disordered graphite associated with defects and amorphous carbon, whereas the G band represents the ordered graphite corresponding to the stretching mode of the C–C bonds in the graphite plane. The D band is assigned to the breathing mode of A_{1g} symmetry due to the phonon interaction near the K zone boundary, while the G band is attributed to the E_{2g} phonon mode of the sp^2 bonded carbon atoms [27–29]. With the calcination temperature rising, Raman spectra undergo significant changes. Specifically, the G band broadened significantly and displayed a shift to higher frequencies (blue shift), G band moved from 1112 cm^{-1} to 1154 cm^{-1} and the D band D peak intensity increased from

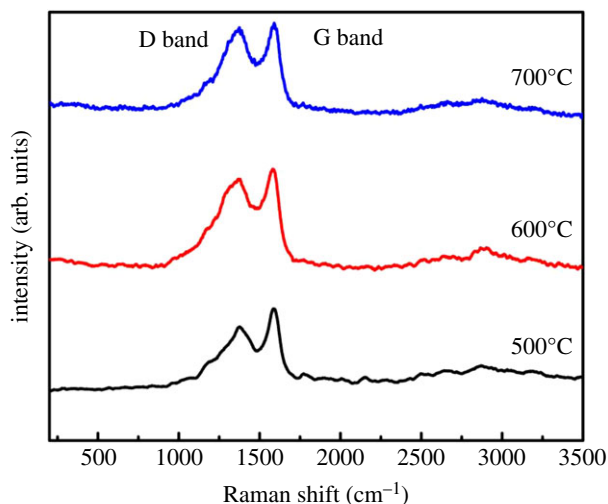


Figure 4. Raman spectra of $\text{Cu}_2\text{O}/\text{HCFs}$. Those were prepared at 400, 500 and 600°C for $\text{Cu}_2\text{O}/\text{HCFs}$.

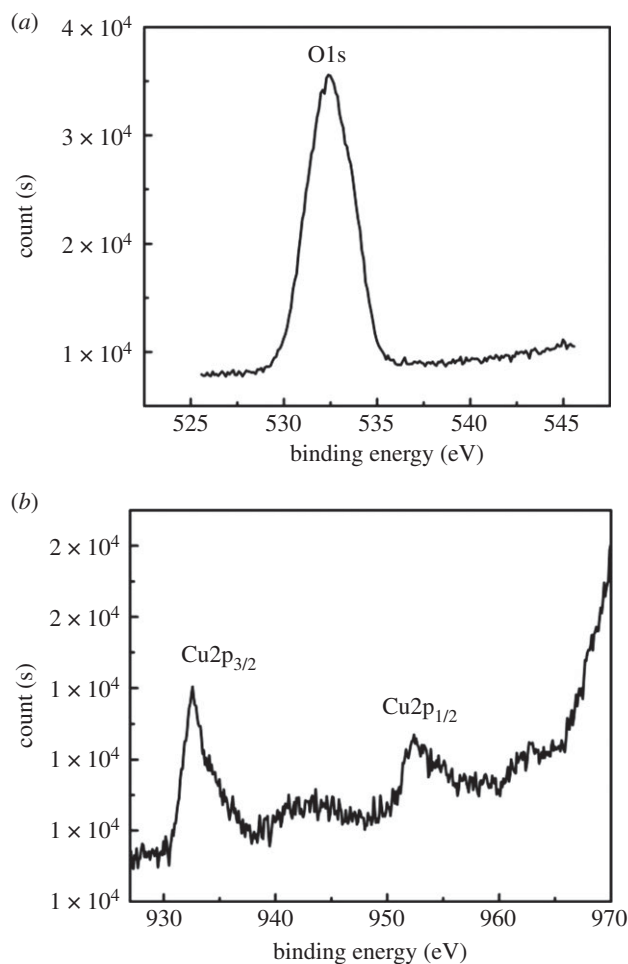


Figure 5. XPS spectra of $\text{Cu}_2\text{O}/\text{HCFs}$. (a) O1s, (b) $\text{Cu}2p_{3/2}$ and $\text{Cu}2p_{1/2}$.

151.03 to 178.71. At 600°C, the peak Intensity ratio (I_G/I_D) was 1.22, crystalline carbon content gradually increases and indicates that the amorphous carbon transforms into graphitized carbon, which is consistent with the XRD results.

Figure 5a,b is O1s and Cu2p X-ray energy spectrum, respectively. As can be seen from figure 5a, the peak at 532.38 eV was assigned to O1s of Cu_2O . As we know, the binding energy of O1s in the crystal lattice is 528.5–529.7 eV, and the binding energy of absorbed oxygen is 530.54–533.77 eV [30]. Owing

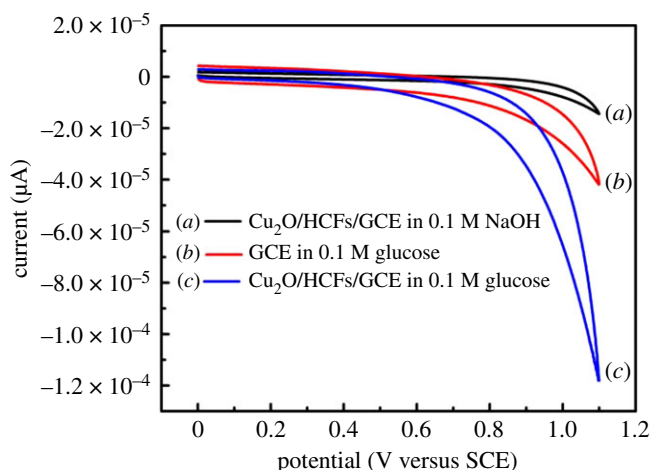
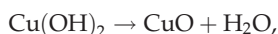
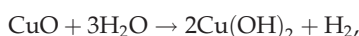


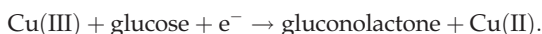
Figure 6. The CV curves of different condition at 100 mV s^{-1} (a) $\text{Cu}_2\text{O}/\text{HCFs}/\text{GCE}$ in the NaOH base solution, (b) the bare GCE in the NaOH solution containing 0.1 M glucose, (c) $\text{Cu}_2\text{O}/\text{HCFs}/\text{GCE}$ in the NaOH solution containing 0.1 M glucose.

to the combination of copper and oxygen in the precursor, the O1s peak appears in figure 5a. As shown in figure 5b, the peaks at 932.58 and 953.38 eV were, respectively, assigned to $\text{Cu}2\text{p}_{3/2}$ and $\text{Cu}2\text{p}_{1/2}$ of Cu_2O , suggesting the presence of Cu_2O [31]. It is reported in the literature that a satellite peak in the XPS spectrum of $\text{Cu}2\text{p}$ indicates the presence of $\text{Cu}(\text{II})$ in the sample, unobvious satellite peaks appear in the figure 5b, of $\text{Cu}(\text{II})$ in the sample, unobvious satellite peaks appear in figure 5b, this means the presence of low content of $\text{Cu}(\text{II})$ in the sample [32]. The results of XPS are in consistent with the observation from XRD, it is further explained that the metal nanoparticles in the material are mainly Cu_2O particles.

To investigate the electrochemical properties of $\text{Cu}_2\text{O}/\text{HCFs}$, the CV studies were performed in glucose solution at a scan rate of 100 mV s^{-1} and potential range from 0 to +1.1 V concerning the electrode. Zhang *et al.* [33] investigated the effect of pH value on the glucose electrochemical oxidation by $\text{Cu}_2\text{O}/\text{HCF}$ -modified electrode. The result showed that it is helpful to the mutarotation of glucose at high pH value and increasing current. Because glucose is easily oxidized under alkaline conditions, we choose 0.1 M NaOH for non-enzymatic glucose detection. Figure 6a–c severally displays the cyclic voltammograms (CVs) of the bare GCE, $\text{Cu}_2\text{O}/\text{HCFs}/\text{GCE}$ in 0.1 M NaOH with and without the presence of glucose at room temperature; a is the CV curve of $\text{Cu}_2\text{O}/\text{HCFs}/\text{GCE}$ in the blank NaOH base solution, b is the CV curve of the bare GCE in the NaOH solution containing 0.1 M glucose and c is the CV curve of the $\text{Cu}_2\text{O}/\text{HCFs}/\text{GCE}$ in the NaOH solution containing 0.1 M glucose. From curves b and c, it can be seen that an oxidation process started at ca +0.5 V and reached a peak at about +1.1 V on the modified electrodes, but the modified electrode has the more obvious electrochemical response to glucose. Comparing a and b curves, while no peak has been observed in the CV curve in the absence of glucose, a dramatic change was observed at the electrode when glucose was added. Anodic peak current of $\text{Cu}_2\text{O}/\text{HCFs}/\text{GCE}$ apparently enlarged at 0.8 V. This illustrated that the $\text{Cu}_2\text{O}/\text{HCFs}/\text{GCE}$ have the electrochemical ability of glucose oxidation, which corresponded to the irreversible glucose oxidation due to the conversion of $\text{Cu}(\text{II})$ to $\text{Cu}(\text{III})$. The possible reaction could be explained by the following equations:



and



$\text{Cu}(\text{III})$ is generated on the Cu_2O surface rapidly and the oxidized glucose is converted to gluconic acid. Also, the conversion of $\text{Cu}(\text{III})$ into $\text{Cu}(\text{II})$ species gives rise to the increase in the oxidation peak current and the decrease in the reduction peak current [34]. The formation of $\text{Cu}(\text{III})$ species not only leads to high catalytic activity but also plays the role of an electron transfer mediator. Moreover, the cubic Cu_2O has the characteristics of the large specific surface area and is conducive to electrochemical reactions [35]. Figure 7 shows Nyquist plots for Faradic impedance measurement of bare GCE (red curve) and $\text{Cu}_2\text{O}/\text{HCFs}/\text{GCE}$ (black curve) in 0.1 mol l^{-1} NaOH containing 10 mmol l^{-1}

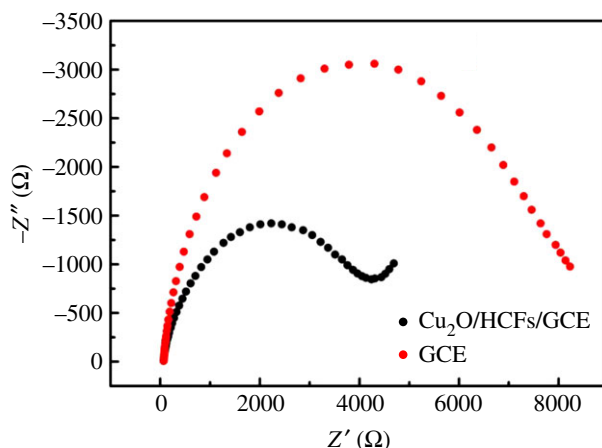


Figure 7. Nyquist plots for Faradic impedance measurement of bare GCE (red curve) and $\text{Cu}_2\text{O}/\text{HCFs}/\text{GCE}$ (black curve) in 0.1 mol l^{-1} NaOH containing 10 mmol l^{-1} $\text{K}_3[\text{Fe}(\text{CN})_6]/\text{K}_4[\text{Fe}(\text{CN})_6]$. The frequency range is from 0.01 Hz to 100 kHz and the amplitude is 0.21 mV.

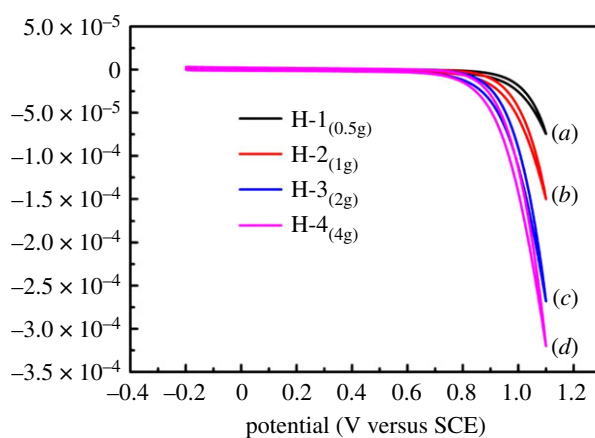


Figure 8. The CV curves of different products at 100 mV s^{-1} in the 0.1 M NaOH solution containing 0.1 M glucose. (a–d) is the curve of H-1, H-2, H-3 and H-4 samples, respectively.

Table 1. The amount of Cu in the products.

| sample | content of Cu in the products (wt%) |
|--------|-------------------------------------|
| H-1 | 7.43 |
| H-2 | 13.00 |
| H-3 | 20.65 |
| H-4 | 22.52 |

$\text{K}_3[\text{Fe}(\text{CN})_6]/\text{K}_4[\text{Fe}(\text{CN})_6]$. The frequency range is from 0.01 Hz to 100 kHz and the amplitude is 0.21 mV. When the electrode was modified with $\text{Cu}_2\text{O}/\text{HCFs}$, the diameter of the semicircle became significantly smaller, indicating that $\text{Cu}_2\text{O}/\text{HCFs}$ can effectively accelerate the transmission of electrons on the electrode surface. The results of the electrochemical impedance spectroscopy (EIS) of the glassy carbon electrode and the modified electrode are consistent with the results of CV.

The Cu contents of the H-1, H-2, H-3 and H-4 samples were obtained by ICP-MS, and the amounts of Cu in the products are listed in table 1. The relationship between the peak current value and the contents of copper was analysed. It can be seen from table 1 that as the content of copper acetate in the precursor increases, the content of Cu in the sample is also increasing, but the content of Cu does not increase linearly. When the mass of copper acetate in the precursor is increased from 0.5 g to 2 g, the content of Cu in HCFs changes obviously. When the mass of copper acetate in the precursor is increased from

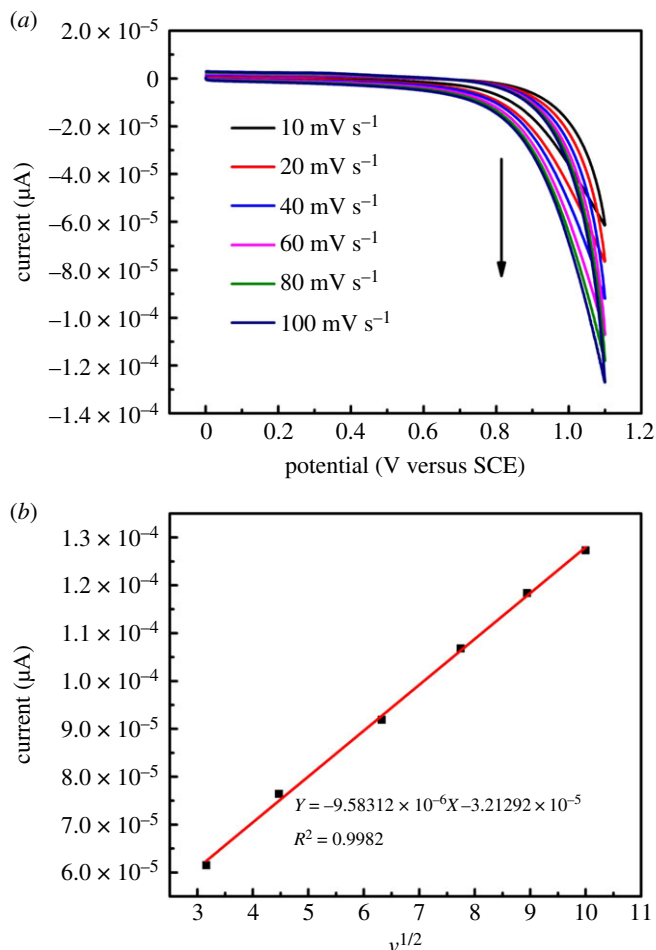


Figure 9. (a) CVs of the Cu₂O/HCFs/GCE in the 0.1 M NaOH solution with 5.0 mM of glucose at different scan rates (10, 20, 40, 60, 80, 100 mV s⁻¹, respectively). (b) The linear dependence of oxidation peak current with the scan rate.

2 g to 4 g, the content of Cu in MHCFs is no longer changed obviously. This coincides with the change in the peak current of figure 8. The reason is that the content of glucose is reducing; however, the content of glucose in the precursor is constant, and its reducing ability is also limited, only a certain amount of copper acetate can be reduced, therefore, according to the data from table 1, the optimum doping amount of copper acetate is 2 g.

To further discuss the electrochemical properties, the CVs of Cu₂O/HCFs electrode at different scan rates ranging from 10 to 100 mV s⁻¹ in the potential window of 0–1.1 mV in the 0.1 M NaOH solution containing 1.0 mM glucose. The oxidative peak current increased with the increasing scan rate in the range of 10–100 mV s⁻¹, as shown in figure 9a. A linear relationship with a linear regression equation

$$I(A) = -9.58 \times 10^{-6}v - 3.21 \times 10^{-5} \quad (R^2 = 0.9982),$$

between the oxidation peak current of glucose and the square root of scan rate is observed, as shown in figure 9b. From the results we have obtained, one can conclude that the electrochemical kinetic is controlled by the adsorption of glucose. Figure 10a illustrates the amperometric responses of the Cu₂O/HCFs/GCE upon successive addition of various concentrations (7.99–33.33 μM) of glucose at a work potential of 1.1 V. To achieve a homogeneous glucose concentration instantly, the solution was vigorously stirred to ensure good distribution of electrolyte and glucose. Upon the addition of glucose, the Cu₂O/HCFs/GCE reached the dynamic equilibrium within 6 s, indicating a very fast amperometric response of the modified electrodes. Figure 10b shows the calibration curve of different concentrations of glucose on the modified electrodes. As can be seen from figure 10b, the Cu₂O/HCFs-modified electrode displays a good linear range from 7.99 to 33.33 μM and the linear regression equation can be expressed as

$$I = 8.6538 \times 10^{-8}C - 4.2746 \times 10^{-5} \quad (R^2 = 0.9919),$$

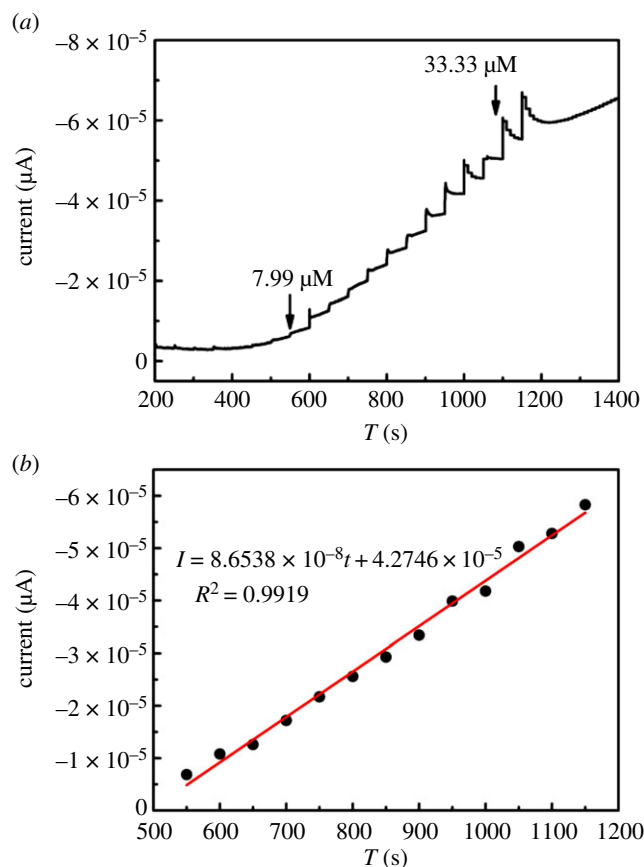


Figure 10. (a) Amperometric responses of the $\text{Cu}_2\text{O}/\text{HCF}$ -modified electrode after successive injection of 40 mM glucose in the 0.1 M NaOH solution at the applied potential of 1.1 V. (b) Plot of the catalytic current versus glucose concentration.

where I and C represent the response current and glucose concentration, respectively. With a high sensitivity of $1218.3 \mu\text{A cm}^{-2} \text{mM}^{-1}$, the low limit of detection (LOD) was $0.48 \mu\text{M}$ by $S/N = 3$, where S and N are the standard deviation of the background current and slope of the calibration curve, respectively. Obviously, the $\text{Cu}_2\text{O}/\text{HCF}$ s-modified electrode here possesses favourable analytical properties. The high sensitivity was attributed to the high electrocatalytic activity of Cu_2O nanoparticles.

To evaluate the selectivity of the $\text{Cu}_2\text{O}/\text{HCF}$ s/GCE, seven possible interfering biomolecules, threonine, valine, lysine, glutamic acid, ascorbic acid (AA), urea and NaCl, which normally coexist with glucose in human blood were examined. The experimental results are shown in figure 11. Taking into consideration that the concentration of glucose is at least 30 times that of AA, NaCl, urea, valine, threonine and lysine, which is much higher than the concentrations of interfering species in human blood [36], thus, normal physiological levels of glucose (0.1 mM), AA (0.01 mM) and NaCl (0.01 mM), urea (0.01 mM), valine (0.01 mM), threonine (0.01 mM), lysine (0.01 mM), in 0.1 M NaOH solution by CV measurement. As can be seen from figure 11, our fabricating sensor demonstrates high selectivity and reliable anti-interference property by comparing the amperometric responses of other relevant electroactive species.

It is well known that the reproducibility and stability are also two important parameters for electrochemical sensors. The experimental results are shown in table 2. The reproducibility experiment of the $\text{Cu}_2\text{O}/\text{HCF}$ s/GCE was carried out in the 0.1 M NaOH solution by adding 0.1 mM glucose and measuring the current responses. In a series of five different electrodes prepared under the same condition, the relative standard deviation (RSD) is 5.64%, indicating that the $\text{Cu}_2\text{O}/\text{HCF}$ s/GCE can hence be a repeated preparation. The storage stability was evaluated at intervals by the measurement toward 0.1 mM glucose in the 0.1 M NaOH solution, and the electrode was stored at room temperature when not in use. The proposed $\text{Cu}_2\text{O}/\text{HCF}$ s/GCE retained about 89.73% of its initial response after 10 days, indicating the $\text{Cu}_2\text{O}/\text{HCF}$ s/GCE has a relatively stable electrochemical performance. Therefore, the $\text{Cu}_2\text{O}/\text{HCF}$ we prepared is an excellent candidate for the fabrication of stable, sensitive and specific sensors for the non-enzymatic detection of glucose.

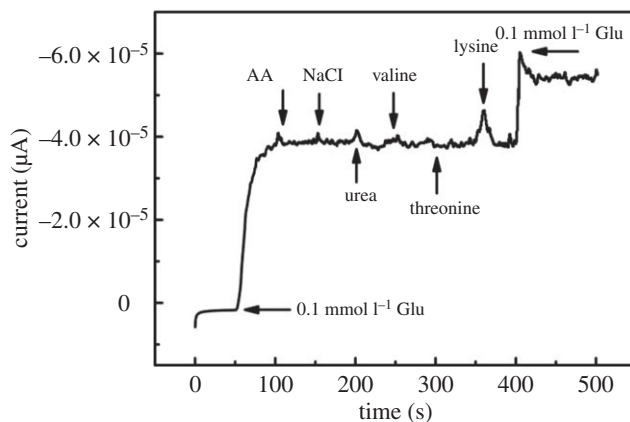


Figure 11. Amperometric responses of the $\text{Cu}_2\text{O}/\text{HCFs}$ -modified electrode to successive additions of glucose (0.1 mM), AA (0.01 mM) and NaCl (0.01 mM), urea (0.01 mM), valine (0.01 mM), threonine (0.01 mM), lysine (0.01 mM) in 0.1 M NaOH.

Table 2. The current responses of reproducibility and repeated experiment.

| performance testing | 1 | 2 | 3 | 4 | 5 |
|----------------------|------------------------|------------------------|------------------------|------------------------|------------------------|
| stability experiment | 1.269×10^{-4} | 1.272×10^{-4} | 1.270×10^{-4} | 1.284×10^{-4} | 1.278×10^{-4} |
| repeated experiment | 1.416×10^{-4} | 1.339×10^{-4} | 1.327×10^{-4} | 1.295×10^{-4} | 1.269×10^{-4} |

4. Conclusion

In summary, we have presented the fabrication of Cu_2O NPs-doped one-dimensional carbon hollow nanomaterial $\text{Cu}_2\text{O}/\text{HCFs}$ via thermal decomposition of a mixture of glucose and CuAc_2 inside cylindrical nano-channels of the AAO template and further carbonization. The photos of SEM and TEM indicate that the diameter of the carbon hollow nanomaterials is about 60 nm, which is in accord with the size of the pores in the AAO templates. The $\text{Cu}_2\text{O}/\text{HCFs}$ can be explained. The XRD patterns that demonstrate Cu_2O NPs have the face-centred cubic lattice. The $\text{Cu}_2\text{O}/\text{HCFs}/\text{GCE}$ show a wide linear range from 7.99 to 33.33 μM with a high sensitivity of $1218.3 \mu\text{A cm}^{-2} \text{mM}^{-1}$ and a detection limit down to 0.48 μM for glucose. The interfering species commonly presenting in the environment have no obvious effect on the oxidation of glucose on the $\text{Cu}_2\text{O}/\text{HCFs}$. Owing to the ease of synthesis, good reproducibility and stability, $\text{Cu}_2\text{O}/\text{HCFs}$ become the promising microstructures for electrochemical biosensor devices of glucose.

Data accessibility. The datasets supporting this article have been uploaded as a part of the electronic supplementary material.

Authors' contributions. Y.L. is responsible for the examination of the thesis topic and the arrangement of the entire experimental project. R.C. is responsible for the operation of the entire experiment, the writing of the first draft of the paper and the analysis of the data. R.L. is the corresponding author of the article. L.G. is responsible for the revision of the article language. S.Q. is responsible for the use of the instrument.

Competing interests. We declare we have no competing interest.

Funding. We gratefully acknowledge the support of this research by the Fundamental Research Funds in Heilongjiang Provincial Universities (no. 135209216).

Acknowledgements. I am grateful to Mr Shuren Liu for guiding my thesis writing. Miss Lihua Zhu's encouragement was very useful to me. Mr Qiang Dai, Miss Yimin Tang and Miss Xue Li helped me to complete the experiment.

References

- Li J, Tu D-h, Li Y, Wang W, Yu Q, Yang J, Lu J. 2018 Co-N-doped carbon nanotubes supported on diatomite for highly efficient catalysis oxidative carbonylation of amines with CO and air. *Appl. Catal. A* **549**, 112–116. (doi:10.1016/j.apcata.2017.09.030)
- Yin ZZ *et al.* 2018 Highly sensitive and selective sensor for sunset yellow based on molecularly imprinted polydopamine-coated multi-walled

- carbon nanotubes. *Biosens. Bioelectron.* **100**, 565–570. (doi:10.1016/j.bios.2017.10.010)
3. Uddin K, Amirul Islam M, Mitra S, Lee J-b, Thu K, Saha BB, Koyama S. 2018 Specific heat capacities of carbon-based adsorbents for adsorption heat pump application. *Appl. Therm. Eng.* **129**, 117–126. (doi:10.1016/j.applthermaleng.2017.09.057)
 4. Tans SJ, Verschueren ARM, Dekker C. 1998 Room-temperature transistor based on a single carbon nanotube. *Nature* **393**, 49–52. (doi:10.1038/29954)
 5. Bachtold A, Hadley P, Nakanishi T, Dekker C. 2001 Logic circuits with carbon nanotube transistors. *Science* **294**, 1317–1320. (doi:10.1126/science.1065824)
 6. An H, Pan L, Cui H, Zhou D, Wang B, Zhai J, Li Q, Pan Y. 2015 Electrocatalytic performance of Pd nanoparticles supported on TiO₂-MWCNTs for methanol, ethanol, and isopropanol in alkaline media. *J. Electroanal. Chem.* **741**, 56–63. (doi:10.1016/j.jelechem.2015.01.015)
 7. Zhang YY, Qing-Feng YI, Chu H, Nie HD. 2017 Catalytic activity of Pd-Ag nanoparticles supported on carbon nanotubes for the electro-oxidation of ethanol and propanol. *J. Fuel Chem. Technol.* **45**, 475–483. (doi:10.1016/S1872-5813(17)30026-9)
 8. Halperin WP. 1986 Quantum size effects in metal particles. *Rev. Mod. Phys.* **58**, 533–606. (doi:10.1103/RevModPhys.58.533)
 9. Dasireddy VDBC, Likozar B. 2018 Selective photocatalytic oxidation of benzene to phenol using carbon nanotube (CNT)-supported Cu and TiO₂ heterogeneous catalysts. *J. Taiwan Inst. Chem. Eng.* **82**, 331–341. (doi:10.1016/j.jtice.2017.11.011)
 10. Liu Z, Xing H, Liu Y, Wang H, Jia H, Ji X. 2018 Hydrothermally synthesized Zn ferrite/multi-walled carbon nanotubes composite with enhanced electromagnetic-wave absorption performance. *J. Alloys Compd.* **731**, 745–752. (doi:10.1016/j.jallcom.2017.09.317)
 11. Sun J, Zan P, Yang X, Ye L, Zhao L. 2016 Room-temperature synthesis of Fe₃O₄/Fe-carbon nanocomposites with Fe-carbon double conductive network as supercapacitor. *Electrochim. Acta* **215**, 483–491. (doi:10.1016/j.electacta.2016.08.139)
 12. Chung K-H, Jeong S, Kim B-J, Kim J-S, Park Y-K, Jung S-C. 2018 Development of hydrogen production by liquid phase plasma process of water with Ni-TiO₂/carbon nanotube photocatalysts. *Int. J. Hydrog. Energy* **43**, 5873–5880. (doi:10.1016/j.ijhydene.2017.09.065)
 13. Tang H, Liu X, Xiao M, Huang Z, Tan X. 2017 Effect of particle size and morphology on surface thermodynamics and photocatalytic thermodynamics of nano-Cu₂O. *J. Environ. Chem. Eng.* **5**, 4447–4453. (doi:10.1016/j.jece.2017.08.034)
 14. Zhou J-H, Zhao J-P, Wu L-K, Hu J-M. 2016 Localized electro-reduction of p-type Cu₂O by SECM under light irradiation. *Electrochem. Commun.* **72**, 171–175. (doi:10.1016/j.elecom.2016.10.002)
 15. Yin H, Cui Z, Wang L, Nie Q. 2016 In situ reduction of the Cu/Cu₂O/carbon spheres composite for enzymaticless glucose sensors. *Sens. Actuat. B* **222**, 1018–1023. (doi:10.1016/j.snb.2015.09.047)
 16. Yazid S, Isa IM, Hashim N. 2016 Novel alkaline-reduced cuprous oxide/graphene nanocomposites for non-enzymatic amperometric glucose sensor application. *Mater. Sci. Eng. C Mater. Biol. Appl.* **68**, 465–473. (doi:10.1016/j.msec.2016.06.006)
 17. Zhou X, Nie H, Yao Z, Dong Y, Yang Z, Huang S. 2012 Facile synthesis of nanospindle-like Cu₂O/straight multi-walled carbon nanotube hybrid nanostructures and their application in enzyme-free glucose sensing. *Sens. Actuat. B* **168**, 1–7. (doi:10.1016/j.snb.2011.12.012)
 18. Yang L, Chu D, Wang L, Wu X, Luo J. 2016 Synthesis and photocatalytic activity of chrysanthemum-like Cu₂O/carbon nanotubes nanocomposites. *Ceram. Int.* **42**, 2502–2509. (doi:10.1016/j.ceramint.2015.10.051)
 19. Shen C, Jia Y, Yan X, Zhang W, Li Y, Qing F, Li X. 2018 Effects of Cu contamination on system reliability for graphene synthesis by chemical vapor deposition method. *Carbon* **127**, 676–680. (doi:10.1016/j.carbon.2017.11.059)
 20. Zhang Y. 2016 One pot synthesis of cuprous oxide nanoparticles on multi-walled carbon nanotubes for nonenzymatic glucose sensors. *Int. J. Electrochem. Sci.* **11**, 8722–8729. (doi:10.20964/2016.10.11)
 21. Han T, Zhou D, Wang H. 2016 The study on preparation and the effect of adsorption over photocatalytic activities of Cu₂O/titanate nanotubes (Cu₂O/TNTs). *Powder Technol.* **301**, 959–965. (doi:10.1016/j.powtec.2016.07.049)
 22. Li J, Jiang J, Xu Z, Liu M, Feng H, Liu Y, Qian D. 2017 Synthesis of a nanocomposite consisting of Cu₂O and N-doped reduced graphene oxide with enhanced electrocatalytic activity for amperometric determination of diethylstilbestrol. *Microchim. Acta* **184**, 4331–4339. (doi:10.1007/s00604-017-2452-4)
 23. Lv R, Zhou W, Shi K, Yang Y, Wang L, Pan K, Tian C, Ren Z, Fu H. 2013 Alumina decorated TiO₂ nanotubes with ordered mesoporous walls as high sensitivity NO(x) gas sensors at room temperature. *Nanoscale* **5**, 8569–8576. (doi:10.1039/c3nr01903a)
 24. Li Y, Zhong Y, Zhang Y, Weng W, Li S. 2015 Carbon quantum dots/octahedral Cu₂O nanocomposites for non-enzymatic glucose and hydrogen peroxide amperometric sensor. *Sens. Actuat. B* **206**, 735–743. (doi:10.1016/j.snb.2014.09.016)
 25. Khan R, Ahmad R, Rai P, Jang L-W, Yun J-H, Yu Y-T, Hahn Y-B, Lee I-H. 2014 Glucose-assisted synthesis of Cu₂O shuriken-like nanostructures and their application as nonenzymatic glucose biosensors. *Sens. Actuat. B* **203**, 471–476. (doi:10.1016/j.snb.2014.06.128)
 26. Lee M, Hong SC, Kim D. 2012 Formation of bamboo-like conducting carbon nanotubes decorated with Au nanoparticles by the thermal decomposition of sucrose in an AAO template. *Carbon* **50**, 2465–2471. (doi:10.1016/j.carbon.2012.01.068)
 27. Qiu Z *et al.* 2018 Ultrahigh level nitrogen/sulfur co-doped carbon as high performance anode materials for lithium-ion batteries. *Carbon* **126**, 85–92. (doi:10.1016/j.carbon.2017.09.100)
 28. Cai J, Liu W, Li Z. 2015 One-pot self-assembly of Cu₂O/RGO composite aerogel for aqueous photocatalysis. *Appl. Surf. Sci.* **358**, 146–151. (doi:10.1016/j.apsusc.2015.08.021)
 29. Huang Y, Yan C-F, Guo C-Q, Lu Z-X, Shi Y, Wang Z-D. 2017 Synthesis of GO-modified Cu₂O nanosphere and the photocatalytic mechanism of water splitting for hydrogen production. *Int. J. Hydrog. Energy* **42**, 4007–4016. (doi:10.1016/j.ijhydene.2016.10.157)
 30. Guo J, Yu H, Dong F, Zhu B, Huang W, Zhang S. 2017 High efficiency and stability of Au–Cu/hydroxyapatite catalyst for the oxidation of carbon monoxide. *RSC Adv.* **7**, 45 420–45 431. (doi:10.1039/c7ra08781k)
 31. Wang L, Zhang R, Zhou T, Lou Z, Deng J, Zhang T. 2016 Concave Cu₂O octahedral nanoparticles as an advanced sensing material for benzene (C₆H₆) and nitrogen dioxide (NO₂) detection. *Sens. Actuat. B* **223**, 311–317. (doi:10.1016/j.snb.2015.09.114)
 32. Sun L, Deng Q, Li Y, Deng L, Wang Y, Ren X, Zhang P. 2016 Solvothermal synthesis of ternary Cu₂O-CuO-RGO composites as anode materials for high performance lithium-ion batteries. *Electrochim. Acta* **222**, 1650–1659. (doi:10.1016/j.electacta.2016.11.155)
 33. Zhang X, Wang G, Zhang W, Wei Y, Fang B. 2009 Fixure-reduce method for the synthesis of Cu₂O/MWCNTs nanocomposites and its application as enzyme-free glucose sensor. *Biosens. Bioelectron.* **24**, 3395–3398. (doi:10.1016/j.bios.2009.04.031)
 34. Niu X, Pan J, Qiu F, Li X, Yan Y, Shi L, Zhao H, Lan M. 2016 Anneal-shrunked Cu₂O dendrites grown on porous Cu foam as a robust interface for high-performance nonenzymatic glucose sensing. *Talanta* **161**, 615–622. (doi:10.1016/j.talanta.2016.09.024)
 35. Wang M, Song X, Song B, Liu J, Hu C, Wei D, Wong C-P. 2017 Precisely quantified catalyst based on in situ growth of Cu₂O nanoparticles on a graphene 3D network for highly sensitive glucose sensor. *Sens. Actuat. B* **250**, 333–341. (doi:10.1016/j.snb.2017.04.125)
 36. Cao H, Yang A, Li H, Wang L, Li S, Kong J, Bao X, Yang R. 2015 A non-enzymatic glucose sensing based on hollow cuprous oxide nanospheres in a Nafion matrix. *Sens. Actuat. B* **214**, 169–173. (doi:10.1016/j.snb.2015.03.026)